The role of ULF waves interacting with oxygen ions at the outer ring current during storm times

B. Yang,[1] Q.-G. Zong,[1,2] S. Y. Fu,[1] X. Li,[3] A. Korth,[4] H. S. Fu,[5] C. Yue,[1] and H. Reme[6]

Received 16 May 2010; revised 26 October 2010; accepted 1 November 2010; published 11 January 2011.

[1] The modulations of the outer ring current O^+ ion fluxes by ULF Pc5 waves are investigated by multisatellite observations during storm times. The O^+ ions have energies up to tens of keV. We concentrate on the process in terms of drift-bounce resonance of O^+ ions with ULF standing waves to understand whether the ring current O^+ ions could be accelerated/decelerated by ULF waves. Two case studies are performed, in which the Cluster satellites travel the outer ring current region in the morning sector with radial distances of about 5.5 R_E. Distinct O^+ ion flux oscillations are observed associated with fundamental mode ULF standing waves. On 25 October 2002, both satellites SC1 and SC4 observe strong poloidal and toroidal standing waves at approximately the same region one by one with a time lag of 45 min. The O^+ ion flux oscillations at around 20 keV are dominantly coherent with the poloidal standing wave at 3.4 mHz with cross phases of near 90° with respect to the magnetic field waves. The O^+ phase space density spectra at 10 to 25 keV, measured by both satellites, deviate significantly from the typical power law distribution. We suggest that the O^+ ions at 10 to 25 keV are accelerated due to drift-bounce resonance with the poloidal standing wave. On 4 November 2002, satellite SC1 observes considerable poloidal and toroidal standing waves. The O^+ ion flux oscillation at around 7 keV is well correlated with both of the two wave modes at 3.7 mHz with cross phases of about 90° with respect to the magnetic field waves. The O^+ spectra at 4 to 8 keV deviates remarkably from the background power law distribution. When satellite SC4 closely encounters the same region 40 min later, the wave activities at 3.7 mHz are found to be rather weak and the O^+ spectra is close to the background power law distribution. We suggest that the spectra variation of SC1 results from the deceleration of O^+ ion at 4 to 8 keV via drift-bounce resonances during the strong wave activities. The observations made in this study reveal the effective role of ULF standing waves in accelerating/decelerating the ring current O^+ ions.

Citation: Yang, B., Q.-G. Zong, S. Y. Fu, X. Li, A. Korth, H. S. Fu, C. Yue, and H. Reme (2011), The role of ULF waves interacting with oxygen ions at the outer ring current during storm times, *J. Geophys. Res.*, *116*, A01203, doi:10.1029/2010JA015683.

1. Introduction

[2] The geomagnetic storm is characterized by a drastic intensification of the ring current. The ions (H^+, O^+, etc.) with energy of tens to hundreds keV (typically 20–200 keV) are thought to be the main carrier of the ring current energy [*Williams*, 1981, 1983, 1985]. It is believed that the H^+ ions are the dominant ion species in the ring current during quiet times, while the O^+ ions become a significant contributor during geomagnetic activities [e.g., *Daglis et al.*, 1999; *Zong et al.*, 2001]. It has been reported that the O^+ ions (1–315 keV) could contributed 30–50% of the total ring current energy density during storm time, compared to less than 3% during quiet times [*Gloeckler et al.*, 1985; *Krimigis et al.*, 1985; *Hamilton et al.*, 1988]. The abundance of O^+ in terms of both number density and energy density increases with increasing geomagnetic activity [*Fu et al.*, 2001]. During extremely large storms, *Nosé et al.* [2005] showed that the O^+ ions were dominant in the magnetotail plasma sheet [*Zong et al.*, 2008] and the O^+/H^+ energy density ratio was as large as 10–20, suggesting more than 90% of the total ring current energy density contributed from O^+ ions. It appears that the source and energization of O^+ ions are more responsive to disturbed activity than H^+ ions.

[1]Institute of Space Physics and Applied Technology, Peking University, Beijing, China.
[2]Center for Atmospheric Research, University of Massachusetts, Lowell, Massachusetts, USA.
[3]Laboratory for Atmospheric and Space Physics, University of Colorado at Boulder, Boulder, Colorado, USA.
[4]Max-Planck-Institut für Sonnensystemforschung, Katlenburg-Lindau, Germany.
[5]Space Science Institute, School of Astronautics, Beihang University, Beijing, China.
[6]Centre d'Etude Spatiale des Rayonnements, University of Toulouse, Toulouse, France.

0148-0227/11/2010JA015683

[3] As the O^+ ions are extremely rare in the solar wind, they are believed to exclusively originate from the ionosphere. The ionospheric outflow O^+ ions (tens of eV) reach to the lobe/plasma sheet region and then convect into the inner magnetosphere, where they form the storm time ring current. It is not well understood how the O^+ ions are accelerated up to ring current energies. One paradigm advocates the effective role of enhanced electric field associated with extended long time period of southward IMF during storm times, while another paradigm emphasizes the important role of substorm process for storm time ring current growth [see *Kamide et al.*, 1998, and reference therein]. It has been suggested that the ionospheric origin of low-energy O^+ ions in the lobe/plasma sheet are strongly accelerated at the magnetic reconnection region (X = −20 to −30 R_E), and are subsequently transported into the near-Earth plasma sheet [*Ipavich et al.*, 1985; *Wilken et al.*, 1995; *Zong et al.*, 1997, 1998]. Also proposed is that the energization of O^+ ions is caused by substorm-associated magnetic field reconfiguration and/or current sheet acceleration [*Delcourt et al.*, 1990; *Sánchez et al.*, 1993; *Nosé et al.*, 2000; *Fok et al.*, 2006; *Nosé et al.*, 2009]. However, it was argued by *Daglis and Axford* [1996] that there existed a direct short-timescale feeding of the magnetosphere with ionospheric ions, indicating the injection of O^+ ions to the ring current region was faster than the traditional concepts as described in the paper by *Kamide et al.* [1998].

[4] On the other hand, the ultralow-frequency (ULF) waves impact the behavior of electrons/ions in the inner magnetosphere remarkably. *Brown et al.* [1968] first reported about modulations of energetic particle fluxes in the minute range, and then followed by extensive observations [e.g., *Kokubun et al.*, 1977; *Baker et al.*, 1980; *Su et al.*, 1980; *Kremser et al.*, 1981; *Takahashi et al.*, 1985, 1990]. The theory of charged particle behavior in ULF waves has been well developed by *Southwood and Kivelson* [1981, 1982]. Due to the comparable periods between the ULF waves and the particle drift motions (radiation belt electrons)/bounce motions (ring current ions, background ion population), drift resonance or drift-bounce resonance can be excited and results in the energy transfer between the waves and particles [e.g., *Elkington et al.*, 2003; *Ozeke and Mann*, 2008]. With the data from the Cluster mission, observational studies of the drift resonance between the radiation belt electrons and the ULF standing waves with periods of several minutes (Pc5 range) have been recently reported [*Zong et al.*, 2007, 2009; *Yang et al.*, 2010]. These studies confirmed the active role of ULF standing waves in accelerating the electrons. However, the modulations of ring current ions, especially of O^+, with ULF standing waves and the presumed acceleration process of these ions have been rarely reported. In contrast, the ring current ions (particular H^+) were always thought to be a free energy source in generating ULF waves in the magnetosphere [e.g., *Hughes et al.*, 1978; *Glassmeier et al.*, 1999; *Wright et al.*, 2001].

[5] The main focus of this paper is to study the ring current O^+ ion modulations associated with ULF standing waves during storm times by multisatellite observations. We concentrate on the O^+ dynamics in terms of drift-bounce resonance, in order to understand whether the ring current O^+ ions could be accelerated/decelerated via resonating with the ULF waves. The observations made in this study suggest that ULF waves can effectively modulate and accelerate/decelerate the ring current O^+ ions.

2. Observations

[6] The data presented in this study are obtained by the Fluxgate Magnetometer (FGM) [*Balogh et al.*, 2001], Electric Field and Wave (EFW) experiment [*Gustafsson et al.*, 2001] and Cluster Ion Spectrometry (CIS) [*Rème et al.*, 2001] on board the Cluster satellites. The FGM and EFW instruments give the spin averaged (4 s) magnetic field and electric field data, respectively. The Composition Distribution Function (CODIF) sensor of the CIS instrument provides the full 3-D distributions of the major ion species (H^+, O^+, He^+, He^{2+}) with energies from 0 to 40 keV/*e*. Further we also examine the particle data obtained from the RAPID (Research with Adaptive Particle Imaging Detectors) instrument [*Wilken et al.*, 2001]. The RAPID spectrometer provides the 3-D suprathermal plasma measurements in the energy range from 20 to 400 keV for electrons, 40 to 1500 keV for protons and helium ions, and 90 to 1500 keV for heavy ions (CNO). The combination of CODIF and RAPID measurements will cover almost the whole ring current energy range [*Williams*, 1981], except for the energy gap between 40 and 90 keV for heavy ions.

[7] We selected two events in which distinct O^+ ion flux oscillations associated with the magnetic and electric ULF standing waves at the same frequency were observed. The Cluster satellites encountered the ring current region near its perigee and were located at a radial distance of about 5.5 R_E. A detailed analysis of these two events is shown below.

2.1. Event A: 25 October 2002

[8] A magnetic storm occurred on 24 October 2002, with a *Dst* index reaching its minimum of −98 nT at 2100 UT. The time interval we are interested is between 1500 and 1700 UT on 25 October 2002, during the storm recovery phase with *Dst* = −68 nT. Observations from the ACE spacecraft showed the IMF Bz was small and positive with an average level of ~3 nT, the solar wind dynamic pressure was around 2 nPa without obvious perturbations, while the flow speed was at a high level with a magnitude of about 700 km/s.

[9] The Cluster satellites were traveling inbound to its perigee from the Southern Hemisphere on the morning side (0920 MLT). The satellite SC1 traveled inbound preceding SC4 by a large distance (~13000 km). Figure 1 gives an overview of the CODIF measurements made by SC1 and SC4. Figure 1a shows the spectrogram of the O^+ ions (6–40 keV) from SC1 between 1520 and 1600 UT on 25 October 2002. Flux oscillations were observed with a period of about 5 min. The pitch angle distribution (PAD) of the O^+ at 15–25 keV is shown in Figure 1b. The periodic pitch angle dispersion-like properties are thought to be a result of the modulations of the ion bounce motions by ULF waves. The spectrogram and PAD data from satellite SC4 between 1605 and 1645 UT are displayed in Figures 1c and 1d, respectively. We find the similar features on SC1. The gray and purple rectangular bars on top Figures 1a and 1c illustrate the time intervals when distinct flux oscillations appear on SC1 and SC4, respectively. In addition, the spectrogram of the CNO ions (mostly O^+)

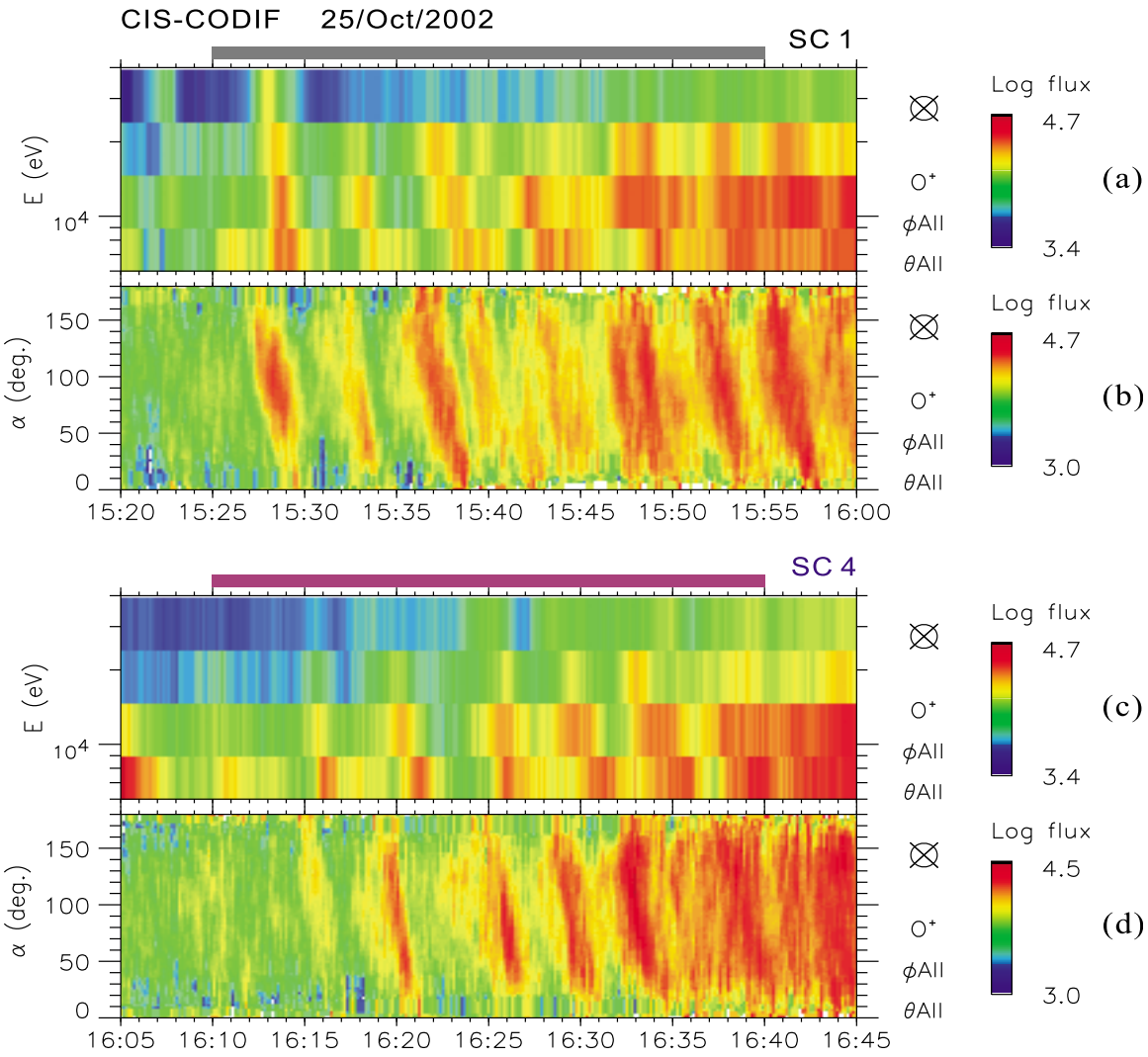

Figure 1. (a) The spectrogram of the O^+ (6 to 40 keV) between 1520 and 1600 UT as obtained from the CODIF instrument on board satellite SC1. (b) The O^+ pitch angle distributions at the energy range of 15 to 25 keV. (c) Same as Figure 1a but from satellite SC4 between 1605 and 1645 UT. (d) Same as Figure 1b but from satellite SC4 between 1605 and 1645 UT.

from 90 to 1500 keV exhibited no visible flux oscillations (not shown here).

[10] Figure 2 shows the satellite orbital information during the corresponding time interval marked by the rectangular bars between 1525 and 1555 UT for SC1 and 1610 and 1640 UT for SC4. The L value variations of SC1 and SC4, derived from the IGRF model, are shown in Figure 2a as black and blue dotted lines, respectively. Figure 2b shows the longitudes (defined as positive eastward with noon at 0°) of SC1 and SC4 in GSM coordinate. The largest azimuthal separation of the two satellites is less than 2°. The L value differences between SC1 and SC4 are within 0.4 between 1535 and 1555 UT (1420 and 1440 UT), although the difference are slightly larger (0.4 to 0.9) between 1525 and 1535 UT (1410 and 1420 UT). We suppose that SC1 and SC4 traveled through approximately the same region with a time lag of 45 min. They both observed the distinct O^+ flux oscillations, suggesting the flux oscillations lasted for at least 75 min at the ring current region with L = 10 to 7.

[11] To analyze the frequency properties of the O^+ fluxes, we apply the fast Fourier transform (FFT) on the flux variations. The resulting normalized power spectral density profiles are shown in Figure 3. The O^+ flux oscillations at both 19.4 keV (solid line) and 11.9 keV (dashed line) exhibit peak wave powers at around 3.4 mHz. These signatures appear on both SC1 (Figure 3a) and SC4 (Figure 3b), indicating the O^+ fluxes at these energies are modulated by a stable wave frequency for hours.

[12] Figure 4 shows the magnetic and electric field measurements from both SC1 and SC4. The electric field component directing along the spin axis is calculated by assuming $\boldsymbol{E} \cdot \boldsymbol{B} = 0$. The local mean field-aligned (MFA) coordinate is applied to study different wave modes [e.g., *Takahashi et al.*, 1990]. In this local system, the parallel unit vector $\boldsymbol{e}_p$ is along the 15 min running average of the magnetic field vector, the azimuthal unit vector $\boldsymbol{e}_a$ is in the direction of $\boldsymbol{e}_p \times \mathbf{r}$, where $\mathbf{r}$ is the position vector of the satellite with respect to the center of the Earth, and then the radial unit vector $\boldsymbol{e}_r$ completes the triad, given by $\boldsymbol{e}_r = \boldsymbol{e}_a \times \boldsymbol{e}_p$.

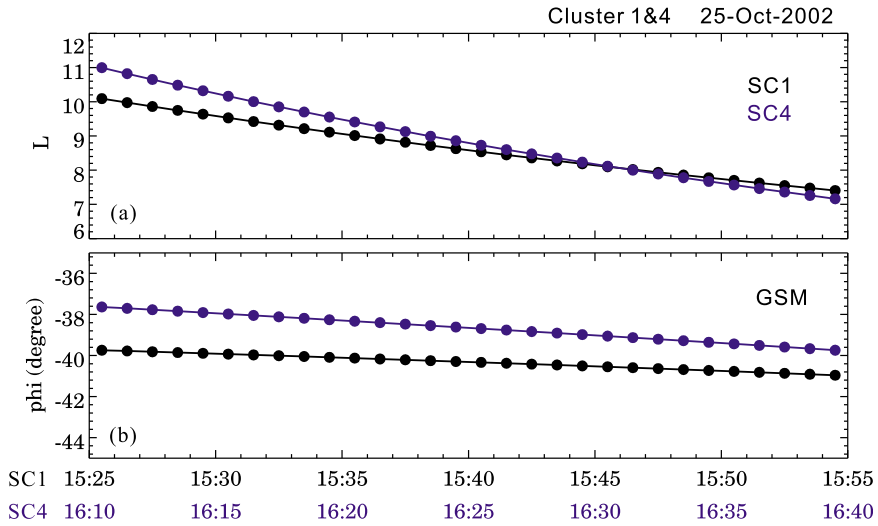

Figure 2. (a) The L value variations of SC1 (black) between 1525 and 1555 UT and SC4 (blue) during 1610–1640 UT, as derived from the IGRF model. The time intervals correspond to the rectangular bars marked in Figure 1. (b) Same as Figure 2a but for the satellite longitudes in GSM coordinate.

[13] Figures 4a and 4b show the magnetic field (blue) and electric field (red) variations of the poloidal and toroidal modes between 1520 and 1600 UT from SC1. The electric fields shown here are obtained by 1 min sliding average to eliminate the high-frequency perturbations. Dynamic power spectrum of the poloidal and toroidal electric field components (raw data without smoothing) are displayed in Figures 4c and 4d. Both the poloidal and toroidal electric fields reveal predominant wave powers at around 3.4 mHz, which are consistent with the main frequency of the O^+ flux oscillations. It is found that the wave power of the toroidal wave at 3.4 mHz is larger than that of the poloidal wave. Further, we perform a band-pass-filtering process on both wave modes with the central frequency at 3.4 mHz and a bandwidth of 1.0 mHz. As shown in Figures 4e and 4f, the magnetic field (blue) and electric field (red) exhibit phase differences of 90° for both wave modes, suggesting they are standing waves along the magnetic field lines [*Singer et al.*, 1982]. Using the stretched string model, the observed poloidal and toroidal waves are determined as the fundamental modes [e.g., *Zong et al.*, 2009]. The results from SC4 between 1610 and 1650 UT are shown in Figures 4g–4l, in the same format as those from SC1. The spectral analysis and filtering process reveal the similar results as those of SC1. The amplitudes of the both poloidal and toroidal waves at 3.4 mHz observed by SC4 are slightly larger than those observed by SC1, indicating the fundamental mode standing waves are even more active after about 45 min. In addition, we should point out that for both satellites, there are essentially no wave oscillations (amplitude less than 4 nT) on the parallel magnetic components, indicating the absence of compressional waves.

[14] The cross wavelet analyses [*Grinsted et al.*, 2004] are performed to investigate the relationship between the O^+ flux oscillations and the poloial/toroidal waves [e.g., *Zong et al.*, 2007]. The squared wavelet coherence of the O^+ flux oscillation at 19.4 keV with the poloidal mode magnetic and electric fields from SC4 are shown in Figures 5a and 5b, respectively. The results for the toroidal mode are presented in Figures 5c and 5d. We notice that the coherence for the magnetic and electric fields belonging to the same wave mode are very similar to each other at their main frequency band, since the magnetic and electric field oscillations are highly coupled for standing waves. It is shown that the O^+ flux is mainly coherent with the poloidal mode (coherence more than 0.9) between 1610 and 1630 UT at the period of around 290 s (i.e., 3.4 mHz). The toroidal mode plays a much weaker role in modulating the O^+ fluxes, although its wave power at 3.4 mHz is about tenfold of the poloidal

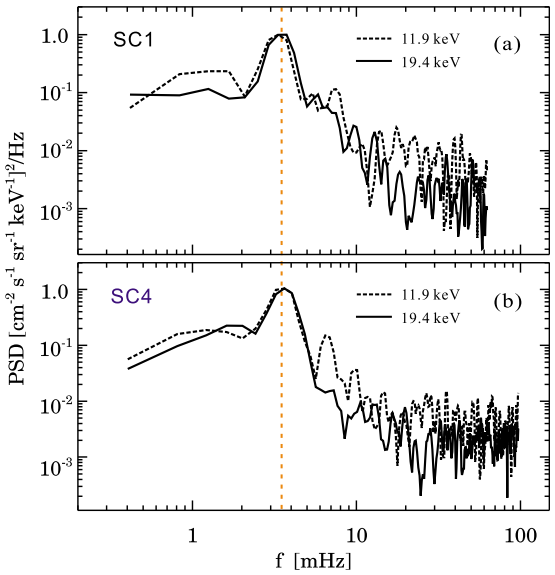

Figure 3. Normalized power spectral density profiles of the O^+ fluxes at the energy channel of 19.4 keV (solid line) and 11.9 keV (dashed line). (a and b) The results from SC1 and SC4, respectively. The peak frequency at 3.4 mHz is marked by the orange dashed line.

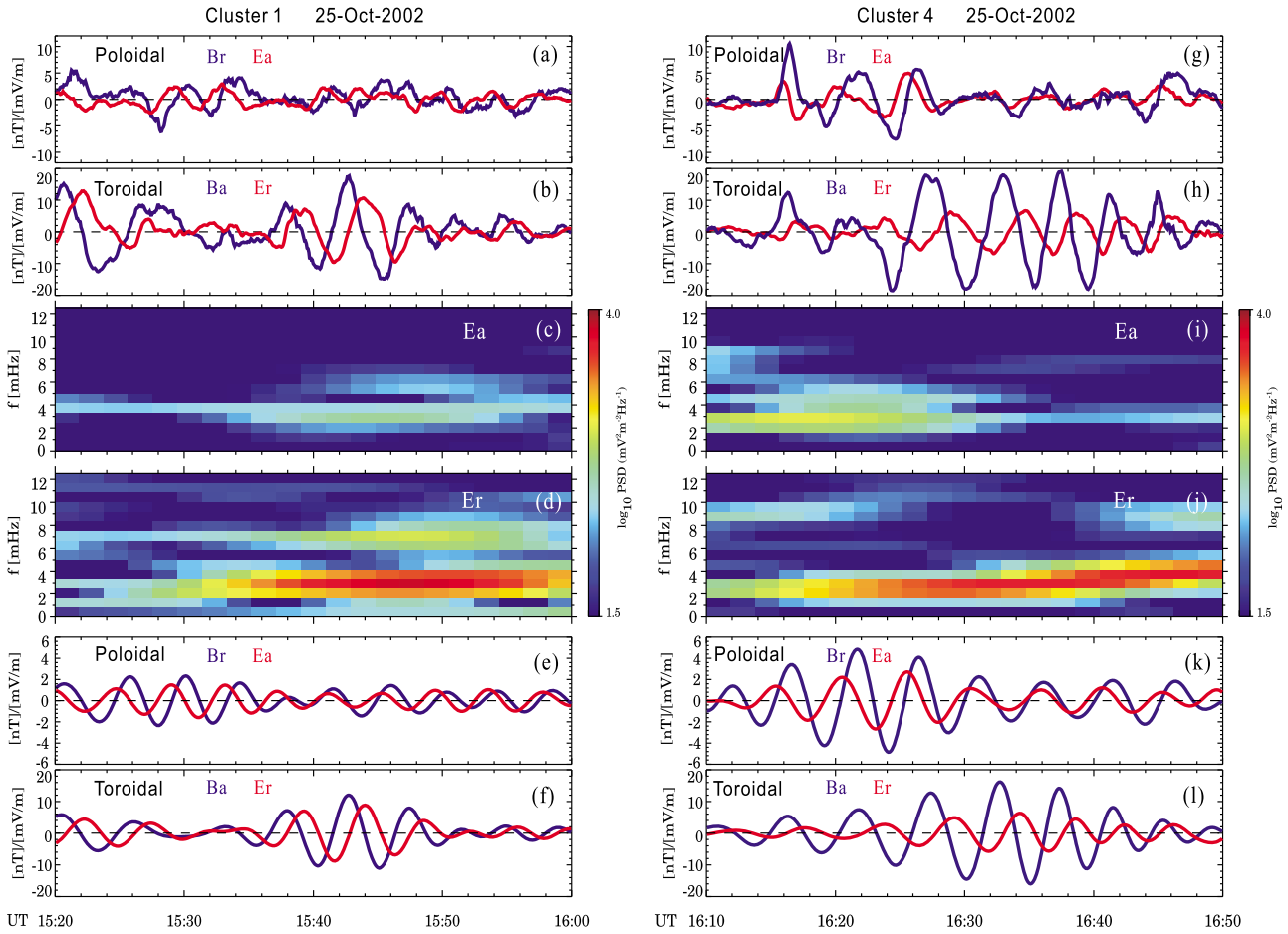

Figure 4. Overview of the magnetic field and electric field measurements from satellite SC1 between 1520 and 1600 UT and SC4 between 1610 and 1650 UT. (a) The radial magnetic field (blue) and azimuthal electric field (red) components of the poloidal mode. (b) The azimuthal magnetic field (blue) and radial electric field (red) components of the toroidal mode. (c) Dynamic power spectrum of the azimuthal electric field. (d) Dynamic power spectrum of the radial electric field. (e) The poloidal magnetic field (blue) and electric field (red) waves at 3.4 mHz, obtained by performing a band-pass filter with 1.0 mHz bandwidth. (f) Same as Figure 4e but for the toroidal mode magnetic field and electric field waves at 3.4 mHz. (g–l) Same as Figures 4a–4f but for the data from satellite SC4.

mode. Furthermore, the relevant cross phases at 3.4 mHz are shown in Figure 5e. It shows a stable phase difference of 90° between the poloidal magnetic field and the O^+ flux oscillation, where the high coherence appears, whereas no stable phase difference is found between the toroidal magnetic field and the O^+ flux oscillations. Furthermore, the cross wavelet analysis is also applied to the observations from SC1 in the same way. We obtain a similar result, that is, the O^+ flux at 19.4 keV is mainly coherent with the poloidal mode between 1525 and 1540 UT with a cross phase of nearly 90° between the poloidal magnetic field and the O^+ flux oscillation.

[15] Figure 6 presents the averaged phase space density (PSD) spectra of O^+ ions (1–40 keV) from SC1 between 1525 and 1555 UT (black) and SC4 between 1610 and 1640 UT (blue). The averages are taken in the time interval of SC1 and SC4 corresponding to the rectangular gray and purple bars marked in Figure 1, respectively, during which the distinct flux oscillations are observed. The vertical error bars denote the standard deviations of the phase space density, as estimated by $\sqrt{N}/N$, where N is the particle counts. The red dashed line shows the typical background spectra with a power law distribution like those commonly observed in the magnetotail [*Sarafopoulos et al.*, 2001]. For both satellites, the O^+ ions from around 10 to 25 keV reveal significant deviations from the power law distribution.

[16] It is estimated that for O^+ ions at 20 keV with an equatorial pitch angle of 10° at L = 9 (around 1620 UT), the bounce frequency is 1.8 mHz (the gradient-curvature drift frequency is much lower, equal to 0.05 mHz), which is comparable to half of the ULF wave frequency (i.e., 3.4 mHz). According to the resonance theory developed by *Southwood and Kivelson* [1982], the observed 90° phase shift of the O^+ flux oscillation at 19.4 keV with respect to the poloidal magnetic field presumably suggests the excitation of the O^+ ion drift-bounce resonance at around 20 keV with the poloidal standing wave. This could give rise to the energy-dependent influence at 10 to 25 keV of

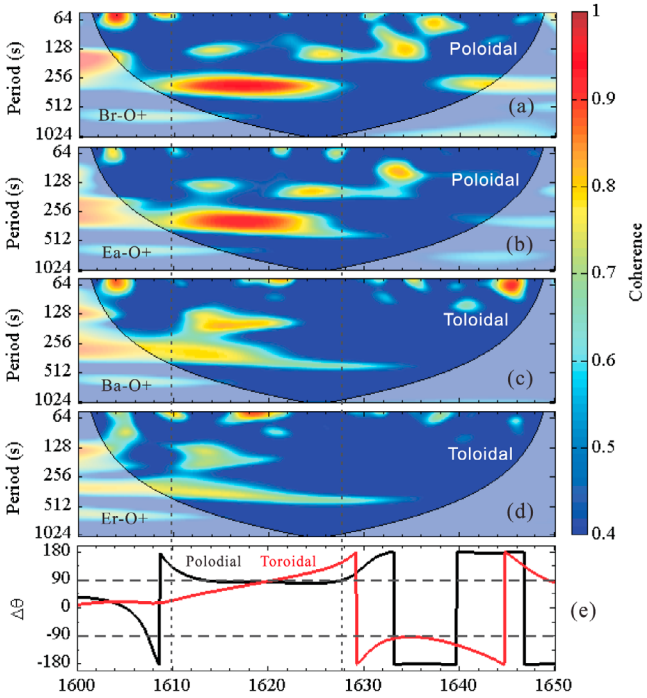

Figure 5. (a) The squared wavelet coherence of the O^+ flux at 19.4 keV with the poloidal mode radial magnetic field component observed by satellite SC4. (b) Same as Figure 5a but for the poloidal mode azimuthal electric field component. (c and d) Same as Figures 5a and 5b but for the toroidal mode azimuthal magnetic field and radial electric field, respectively. (e) The cross phases of the radial (black) and azimuthal (red) magnetic field variations with the O^+ flux at 3.4 mHz, respectively.

the spectra. The theoretical evaluation of the resonant energy will be addressed in section 3.

2.2. Event B: 4 November 2002

[17] This event occurred around 0430–0540 UT on 4 November 2002, during the recovery phase of a moderate storm. The *Dst* index gradually recovered from its minimum of −75 nT at 0700 UT on 3 November 2003 to −60 nT during the time of interest. During this time interval, the IMF Bz was mainly positive with an average level of about 4 nT, the solar wind dynamic pressure was around 2 nPa without remarkable perturbations, and the flow speed was moderate with a magnitude of about 500 km/s.

[18] The Cluster satellites were traveling inbound to its perigee from the Southern Hemisphere on the morning side (0800 MLT). Figure 7 gives an overview of the CODIF measurements from SC1 between 0431 and 0501 UT and SC4 between 0508 and 0538 UT, in the same format as Figure 1. Distinct O^+ flux oscillations and periodic pitch angle dispersion-like properties are observed on SC1 between 0435 and 0451 UT and SC4 between 0512 and 0528 UT, which are marked by the gray and purple rectangular bars on the top Figures 7a and 7c, respectively. It should be noted that high-energy O^+ measurements obtained by RAPID did not show visible flux oscillations in the energy range of 90–1500 keV.

[19] Figure 8 shows the L value and longitude information of the satellites SC1 and SC4 during the time intervals marked by the rectangular bars. The largest azimuthal separation of the two satellites is less than 1° and the largest L value difference is less than 0.4. It is suggested that the two satellites traveled across approximately the same region one by one with a time lag of around 40 min, and the O^+ flux oscillations lasted for at least 1 h at L = 9 to 6.5.

[20] Figure 9 shows the normalized power spectral density profiles of O^+ flux variations at 7.4 keV (solid line) and 4.5 keV (dashed line). The wave powers reach maximum values at around 3.7 mHz on both SC1 and SC4, suggesting the O^+ fluxes at these energies are modulated by a stable wave frequency lasting for at least 1 h.

[21] The magnetic and electric field data are presented in Figure 10, in the same format as Figure 4 except for the data after filtering process. The electric field vector is obtained from the cross product of the magnetic field and the ion bulk velocity measured by the HIA instrument [e.g., *Zong et al.*, 2007]. We should point out that no visible wave oscillations (amplitude less than 3 nT) of the parallel magnetic component appear, suggesting the absence of compressional waves. As shown in Figures 10c and 10d, the electric field components reveal dominant wave powers at around 3.7 mHz in both wave modes from SC1 between 0435 and 0505 UT. We find both the poloidal and toroidal electric field waves are nearly monochromatic and oscillate almost in phase. The wave power of the toroidal magnetic field is about 10 times larger than that of the poloidal magnetic field. As demonstrated in event A, the 90° phase shifts between the magnetic field and the electric field of both wave modes suggest them to be fundamental standing waves. However, it appears rather weak wave activities at

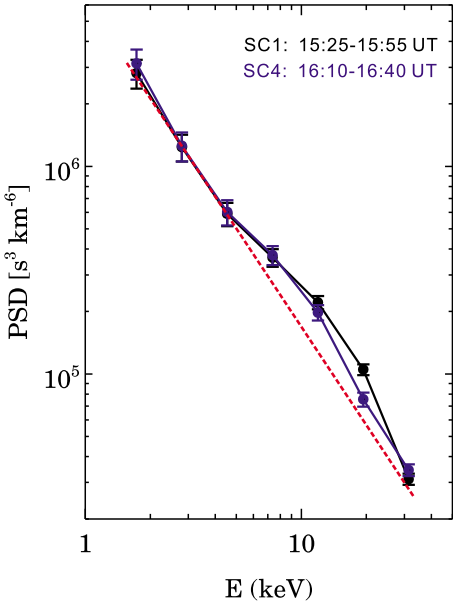

Figure 6. The averaged O^+ phase space density spectra of SC1 (black) and SC4 (blue), respectively. The spectra are averaged over the time periods indicated by the rectangular bars (gray for SC1 and purple for SC4) in Figure 1. The dashed red line indicates the power law fit of the spectra.

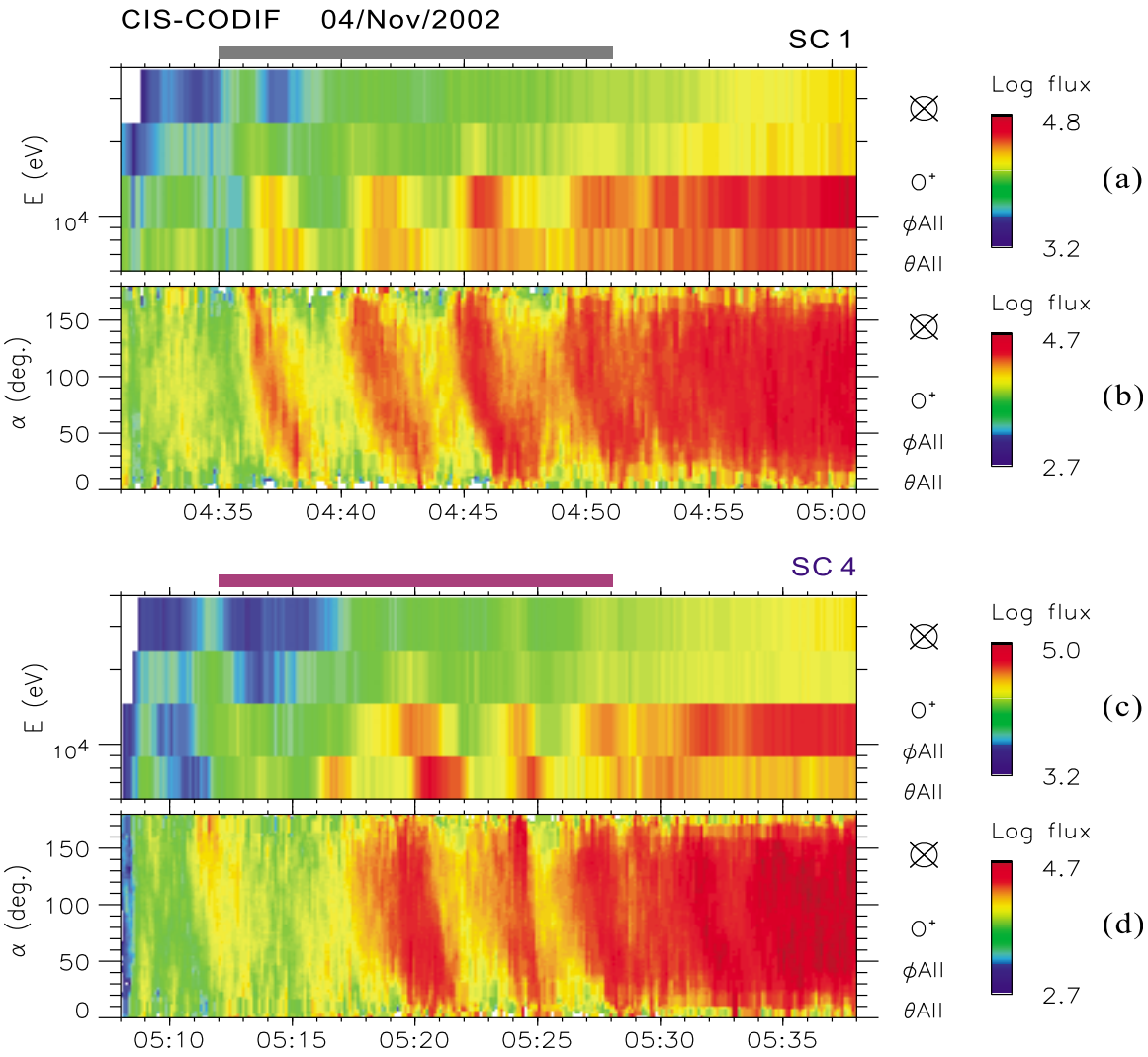

Figure 7. Same as Figure 1 but for the 4 November 2002 event. The O^+ pitch angle distributions are at the energy range of 5 to 20 keV.

3.7 mHz from SC4 between 0515 and 0545 UT, as shown in Figures 10e–10h.

[22] Figure 11 gives the cross wavelet analysis of the O^+ flux at 7.4 keV with the poloidal and toroidal waves, in the same format as Figure 5. The O^+ flux at this energy channel is well coherent with both the poloidal mode and the toroidal mode, with coherence more than 0.8 at the period of around 270 s (i.e., 3.7 mHz) between 0440 and 0455 UT, during which the relevant cross phases are around 90°. This suggests the roles of both the poloidal and toroidal waves to be significant in modulating the O^+ ions in this event. In addition, it should be noted that for satellite SC4, the correlations between the waves at 3.7 mHz and the O^+ flux oscillations are rather weak (less than 0.4).

[23] Figure 12 shows the averaged phase space density spectra of the O^+ ions (1–40 keV) from SC1 between 0435 and 0451 UT (black) and SC4 between 0512 and 0528 UT (blue). The time intervals correspond to the rectangular bars marked in Figure 7. The red dashed line shows a smoothed power law distribution, which closely resembles the spectra of SC4. However, for SC1, it shows a remarkable derivation of the O^+ ions at around 4 to 8 keV from the power law distribution.

3. Discussion

3.1. Wave-Particle Drift-Bounce Resonance and Related Energy Exchange

[24] *Southwood and Kivelson* [1981, 1982] developed a theory of particle drift-bounce resonance with ULF poloidal waves, owning an azimuthally polarized electric field. The drift-bounce resonance condition is given as

$$\omega - m\omega_d = N\omega_b \tag{1}$$

where ω and m are the wave frequency and azimuthal wave number (positive for eastward propagating wave), ω_d and ω_b are the particle drift and bounce frequencies, respectively, and N is an integer which depends on the wave harmonic mode. For the fundamental mode, we have $N = 0, \pm 2, \pm 4, \ldots$.

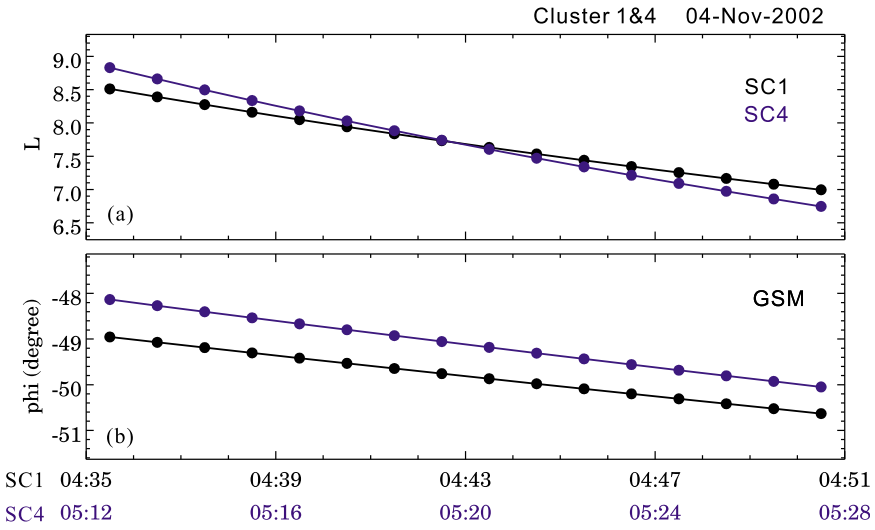

Figure 8. Same as Figure 2 but for the 4 November 2002 event.

[25] The bounce frequency ω_b of ions with energy W (in Joule) in a dipole field is given by [*Hamlin et al.*, 1961]

$$\omega_b = \frac{\pi\sqrt{2W/m_i}}{2LR_E T(\alpha)} \tag{2}$$

For the bounce-average drift frequency ω_d, we use the equation proposed by *Li et al.* [1993] and *Chisham* [1996], which includes both the energy-dependent gradient-curvature term and the electric-field-dependent convection and corotation terms:

$$\omega_d = -\frac{6WLP(\alpha)}{qB_E R_E^2} + \frac{2\psi_0 L^3 \sin\phi}{B_E R_E^2} + \Omega_E \tag{3}$$

The first term of equation (3) indicates the gradient-curvature drift. The second and third terms correspond to the $\boldsymbol{E} \times \boldsymbol{B}$ drift effects due to the convection and corotation electric fields, respectively.

[26] In equations (2) and (3), $T(\alpha)$ and $P(\alpha)$ are given approximately by $T(\alpha) = 1.30 - 0.56 \sin \alpha$ and $P(\alpha) = 0.35 + 0.15 \sin \alpha$ [*Hamlin et al.*, 1961], in which α is the ion's equatorial pitch angle, m_i is the ion mass, L is the McIlwain L shell value [*McIlwain*, 1961], R_E is the Earth's radius, B_E is the equatorial magnetic field strength at the surface of the Earth, ϕ is the azimuthal angle (positive eastward with midnight at 0°), and Ω_E denotes the angular frequency of the Earth's rotation. In addition, ψ_0 is an electric potential indicating the dawn-dusk convection electric fields [*Volland*, 1973; *Stern*, 1975], which is always described as an empirical K_p-dependent function [*Maynard and Chen*, 1975]:

$$\psi_0 = 45\left(1 - 0.159K_p + 0.0093K_p^2\right)^{-3} \tag{4}$$

[27] The energy exchange between the waves and particles through drift-bounce resonance is correlated with the phase space density of the resonant particles, f, as a function of particle energy W and L value. Whether a group of resonant particles contributes to wave growth (particle deceleration) or damping (particle acceleration) depends on the sign of df/dW [*Southwood et al.*, 1969], which is determined as

$$\frac{df}{dW} = \frac{\partial f}{\partial W} + \frac{dL}{dW}\frac{\partial f}{\partial L} \tag{5}$$

If $df/dW > 0$, the particles will lose energy and cause wave growth. Alternatively, if $df/dW < 0$, the particles will gain energy and damp the wave. This equation indicates that the spatial gradient, $\partial f/\partial L$, could contribute to wave growth or wave damping, depending on the sign of dL/dW. Since the

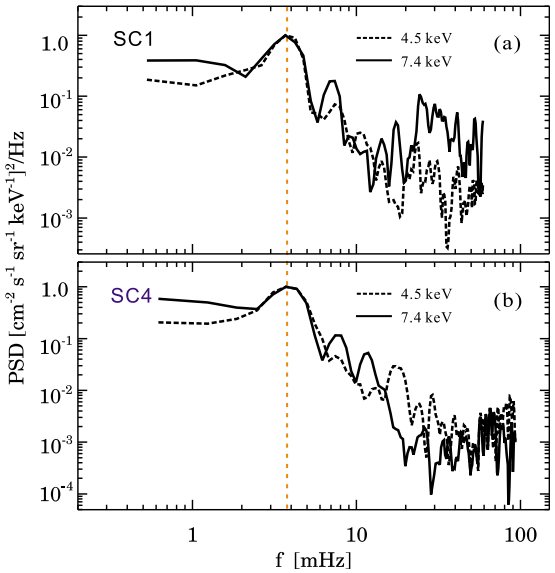

Figure 9. Same as Figure 3 but for the energies at 7.4 keV (solid line) and 4.5 keV (dashed line). The peak frequency at 3.7 mHz is marked by the orange dashed line.

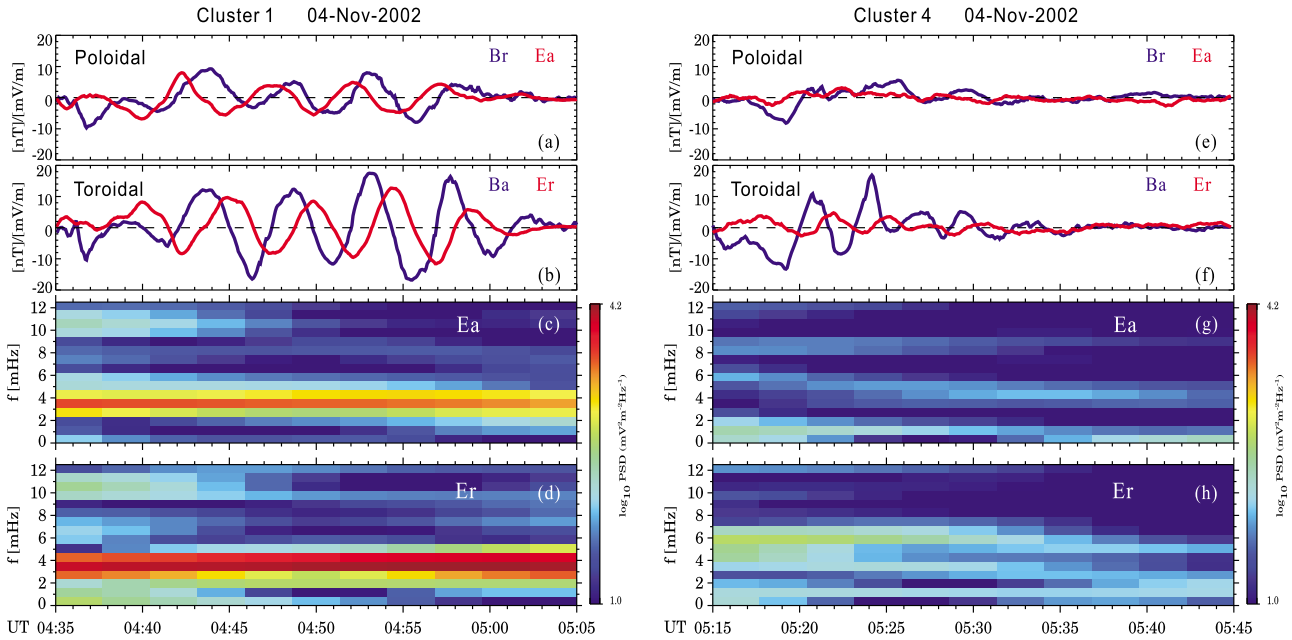

Figure 10. Overview of the magnetic field and electric field measurements from satellite SC1 between 0435 and 0505 UT and SC4 between 0515 and 0545 UT. (a–d) Same as Figures 4a–4d. (e–h) Same as Figures 4g–4j.

Pc5 wave frequency is much lower than the particle gyrofrequency, the quantity dL/dW is proportional to $m/q\omega$ [*Southwood et al.*, 1969].

3.2. Derivation of O^+ Equatorial Pitch Angle

[28] Table 1 shows the magnetic latitudes of the satellites during the corresponding time of interest. Obviously, the Cluster satellites were located in the southern hemisphere for both events. Thus, the observations shown in Figures 1b, 1d, 7b, and 7d indicate the local pitch angles of the O^+ ions at the satellites' locations rather than those at the equator. To evaluate the resonant energy theoretically through the drift-bounce resonance condition, it is essential to know the

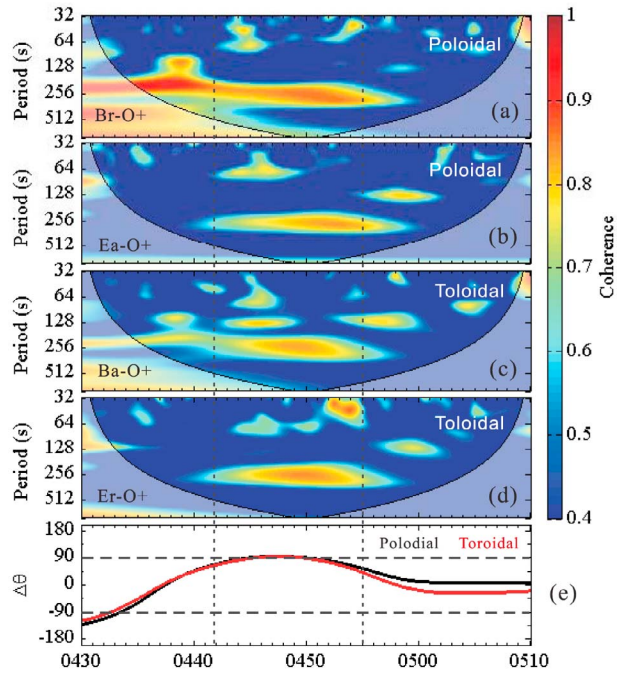

Figure 11. Same as Figure 5 but for the O^+ flux at 7.4 keV observed by satellite SC1 between 0430 and 0510 UT.

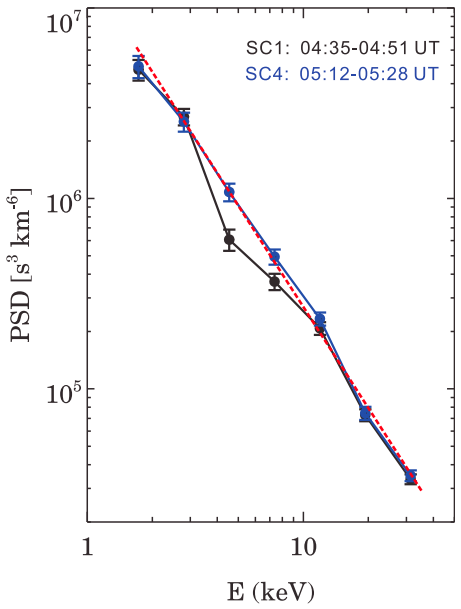

Figure 12. The averaged O^+ phase space density spectra of SC1 (black) and SC4 (blue), respectively. The spectra are averaged over the time periods indicated by the rectangular bars (gray for SC1 and purple for SC4) in Figure 7. The dashed red line indicates the power law fit of the spectra.

Table 1. Magnetic Latitudes of the Satellites During the Corresponding Time of Interest

Event	Satellite	Time (UT)	Magnetic Latitude
A (25 Oct 2002)	SC1	1525–1555	−40° to −30°
	SC4	1610–1640	−46° to −34°
B (04 Nov 2002)	SC1	0435–0455	−38° to −29°
	SC4	0510–0530	−43° to −32°

equatorial pitch angles of the O^+ ions. Although the O^+ flux oscillations appear in a whole range of local pitch angles (0° to 180°), it does not mean that the O^+ ions participating in resonance have a whole range of equatorial pitch angles.

[29] The equatorial pitch angles of O^+ ions participating in resonance cannot be obtained directly from the observations. Instead, we need to deduce the morphology of the ion pitch angle distributions at the equatorial region. *Yang et al.* [2011] have interpreted the formation of these periodic pitch angle dispersion signatures. They are believed to evolve from periodic "in-phase" field-aligned O^+ beams at the equator generated through resonance with ULF waves. To calculate the ion resonant energy based on equation (1), it is appropriate to consider merely the equatorial pitch angles of O^+ ions in the beam structure, because the O^+ ions out of the beam structure are weakly modulated by ULF waves and can be regarded as background population. We then need to calculate the equatorial pitch angle range of the beam structure.

[30] In a simplified way, we assume a dipole field and estimate the ion equatorial pitch angle from its local pitch angle, based on

$$\sin^2 \alpha_{eq} = \sin^2 \alpha_s \frac{\cos^6 \lambda_s}{\left(1 + 3\sin^2 \lambda_s\right)^{1/2}} \tag{6}$$

where α_{eq} is the ion equatorial pitch angle, α_s is the local pitch angle detected by the satellite, and λ_s is the magnetic latitude of the satellite.

[31] For event A (25 October 2002), we get the average magnetic latitude of −40° for satellite SC4 during the time of interest. The equatorial pitch angle (α_{eq} = 21.6°) calculated from α_s = 90° corresponds to the upper limit of α_{eq} in the beam structure. The lower limit of α_{eq} will be 0° as derived from α_s = 0° (or 180°). Nevertheless, the O^+ ions in the beam structure bounced along the field lines periodically due to the modulation by ULF wave. This indicates the O^+ ions participating in resonance should have the lower limit of α_{eq} at least larger than the relevant equatorial loss cone. It is calculated that the equatorial loss cone in a dipole field at L = 9 is about 1.5°. The range of α_{eq} of the O^+ ions in the beam structure is then obtained to be from 1.5° to 21.6°. In addition, we also estimate the result from satellite SC1 with the average magnetic latitude of −35°, which is calculated to be from 1.5° to 27.6°.

[32] In addition, it is possible that the O^+ ions participating in resonance have equatorial pitch angles even larger than the upper limit of α_{eq} we have calculated above. However, these ions should have mirror point latitudes lower than the magnetic latitudes of the satellites. Thus, they cannot be observed by the satellites. Since the aim of calculating the theoretical resonant energy is to make a comparison with the satellite observations, we consider only the equatorial pitch angle range of the O^+ ions observed by the satellites. Therefore, we use the equatorial pitch angle with the range between 1.5° and 27.6°, to calculate the ion resonant energy.

[33] In a similar way, for event B (4 November 2002), the equatorial pitch angle range of the O^+ ions participating in resonance is within 2.3° and 30.2°.

3.3. Theoretical Estimation of O^+ Resonant Energy

3.3.1. Event A (25 October 2002)

[34] The energetic electron flux oscillations at 3.4 mHz were observed by SC1 during 1520–1600 UT and SC4 during 1605–1645 UT, which were believed to be modulated by the ULF standing waves [e.g., *Zong et al.*, 2007; *Yang et al.*, 2010]. It is demonstrated that the electron fluxes are predominantly correlated with the poloidal magnetic field and the electron drift resonances are excited at between 51 and 68 keV, based on the method proposed by *Yang et al.* [2010]. According to the drift resonance condition $\omega = m\omega_d$, the azimuthal wave number of the 3.4 mHz poloidal standing wave is calculated to be $m = 17 \pm 3$, with the wave propagating eastward. We focus on the time between 1613 and 1628 UT for satellite SC4, when the high coherence (>0.9) between the O^+ flux and the poloidal standing wave appears. During this time period, we get the parameters: f = 3.4 mHz, K_p = 3, ϕ = 140° (i.e., 0920 MLT), $L \simeq 9$.

[35] It should be noted that for the O^+ at tens of keV, the term $m\omega_d$ is less than the wave frequency ω but cannot be negligible, while the bounce frequency ω_b is comparable to the wave frequency. Taking into account the fundamental mode, it is feasible to examine N = 2 drift-bounce resonance condition according to equation (1). We then obtain the resonant energy to be within 14.2–34.4 keV. There exists another solution (90–360 keV) satisfying equation (1), which is beyond the energy range of the CODIF instrument (0–40 keV). Though it is covered by the RAPID measurement (90–1500 keV), no visible flux oscillation signatures were observed around this energy range. Thus, we only consider the low-energy solution and compare it with the CODIF observation.

[36] It is worth noting that the wave frequency ω in reality usually has a finite bandwidth rather than "monochromatic." This will cause a spread in resonant energy [e.g., *Takahashi et al.*, 1990], if the particle's equatorial pitch angle is fixed. Alternatively, if the particle's energy is fixed, this will result in a spread in the equatorial pitch angle of the particle participating in resonance. We define the edge of the wave bandwidth as where the wave power decreases to half of its maximum strength [e.g., *Takahashi and Ukhorskiy*, 2007]. From the power spectrum density profile of the poloidal electric field, we obtain the wave bandwidth to be 0.74 mHz. That is, $f = 3.4 \pm 0.37$ mHz. Approximately, according to the resonance condition, the maximum equatorial pitch angle of O^+ ions participating in resonance is 40.2°. It means 46% increase of the upper limit magnitude (27.6°) derived from observations. Meanwhile, from the calculation, the minimum equatorial pitch angle of O^+ ions that could be in resonance is even as low as 0°. However, this minimum value in reality should not be smaller than the equatorial loss cone (1.5°). Therefore, we suggested that the O^+ ions with equatorial

pitch angle from 27.6° to 40.2° could also participate in resonance, although this portion of ions were not observed by satellites.

[37] On the other hand, it is worth noting that the drift-bounce resonance with N = 4, 6.. can also be reasonable. It is suggested that the higher the magnitude of N, the weaker would be the wave-particle interaction [*Southwood et al.*, 1969]. Moreover, we calculate the O^+ energy to be about 3 keV and 1 keV to satisfy the N = 4 and N = 6 drift-bounce resonance conditions, respectively. However, no apparent flux modulations were observed around these energies. In addition, the high-energy solutions are about several to tens of MeV, which are far beyond the energy scope we consider here.

[38] We have demonstrated that both the satellite SC1 and SC4 observe strong poloidal standing waves, which are both well correlated with the O^+ flux oscillations at around 20 keV. Moreover, the O^+ flux oscillations around this energy exhibit cross phases of nearly 90° with respect to the poloidal magnetic field waves. Therefore, we suggest the excitation of drift-bounce resonance of the O^+ ions at around 20 keV with the poloidal standing wave [*Southwood and Kivelson*, 1982]. This paradigm is further confirmed by the consistency between the theoretical calculations and observations. As shown in Figure 6, the spectra of O^+ ions at around 10–25 keV, observed by both satellites, deviate significantly from the typical power law distribution. This suggests the acceleration of O^+ ions at around 10–25 keV, which could be caused by drift-bounce resonances.

3.3.2. Event B (4 November 2002)

[39] In this event, we focus on the time between 0442 and 0454 UT for satellite SC1, when the O^+ flux is both highly coherent with both the poloidal and toroidal magnetic fields and has phase differences of 90° with respect to both wave modes. We get the parameters: $f = 3.7$ mHz, $K_p = 4$, $\phi = 120°$ (i.e., 0800 MLT), $L \simeq 7$. During the time of interest, the energetic electron flux modulations at around 3.7 mHz were also observed. It is estimated that the electron drift resonances are excited at around 94 keV with the poloidal wave, by using the method proposed by *Zong et al.* [2007]. Consequently, the m value of the poloidal wave is derived to be $m = 15 \pm 1$. The resonant energies are then obtained to be within 8.0–13.7 keV and 790–1240 keV to satisfy the N = 2 drift-bounce resonance condition. The low-energy result is fairly consistent with the observed resonant energy around 4–8 keV, although the theoretical result is slightly higher. Nevertheless, for the high-energy result, similar to event A, no visible O^+ flux oscillations were observed around this energy range. Similar to event A, if we consider the effect of the wave bandwidth ($f = 3.7 \pm 0.40$ mHz), the maximum equatorial pitch angle of the O^+ ions participating in resonance is 42.9°, indicating 42% increase of the upper limit magnitude (30.2°) derived from observations. In addition, the minimum equatorial pitch angle should not be smaller than the equatorial loss cone (2.3°), although the calculation indicates this minimum value can be as low as 0°. Thus, we speculate that the O^+ ions with equatorial pitch angle from 30.2° to 42.9° could also participate in resonance.

[40] It is found that both the poloidal and toroidal waves play active roles in terms of resonating with the O^+ ions in this event. *Elkington et al.* [2003] suggested that the toroidal mode with a radially polarized electric field could also resonate with the particles, if the geomagnetic field exhibited an additional noon-midnight asymmetry. This effect of the toroidal mode on energetic electrons was observationally confirmed by *Zong et al.* [2007]. We speculate this effect to be also effective on ring current ions. As shown in Figure 11, the spectra of O^+ ions at around 4–8 keV from SC1 deviates notably from the background power law distribution during strong wave activities. The spectra of SC4 is very close to the power law distribution during rather weak wave activities. Based on the spectra comparison, it is suggested that the O^+ ions at around 4–8 keV are decelerated due to drift-bounce resonances as observed by SC1.

3.4. Comparison With Previous Studies

[41] Previous studies have reported satellite and ground-based observations of ULF waves associated with the unstable ring current protons [e.g., *Hughes et al.*, 1978; *Glassmeier et al.*, 1999; *Wright et al.*, 2001]. They suggested that the drift-bounce resonance of these protons with non-Maxwellian distribution be responsible for the generation of the observed ULF waves. However, they did not investigate the behavior of the O^+ ions, which were thought to be more dynamic than protons during storm times [*Daglis et al.*, 1999]. In this study, we primarily focus on the dynamics of the ring current O^+ ions in interacting with the ULF waves. Also observed in the two events are periodic modulations of the bouncing H^+ ions at hundreds of eV with the same ULF waves. They are demonstrated by *Yang et al.* [2010] and will not be discussed here.

[42] *Williams* [1981] estimated that the bulk (~90%) of the ring current is at the energy range of 15–250 keV, if they are all assumed to be protons, and the mean energy of the ring current was several tens of keV. It should be noted that for the same energy and differential flux, the contribution of the O^+ ions to the energy density is 4 times larger than that of protons. Based on the ion flux measurements from both the CODIF and RAPID instruments, we estimate that the O^+ ions at 1–40 keV account for 30% to 40% of the whole energy density contributed from the O^+ ions covering energy range from 1 to 500 keV. Moreover, if the total ring current energy density is supposed to be made by both the O^+ and H^+ at the energy range of 1–500 keV, the contribution of the O^+ ions at 1–40 keV amount to about 15% of the total energy density. Thus, the low-energy tail of the ring current O^+ ions (1–40 keV) we studied here are within the major ring current energy range.

[43] It is suggested that O^+ ions at the resonant energy (around 10–25 keV in event A and 4–8 keV in event B) were accelerated in event A (25 October 2002) and decelerated in event B (4 November 202) through drift-bounce resonances with the ULF standing waves. Although the acceleration/deceleration effect on the O^+ ions at tens of keV might be weak and not as significant as the radiation belt electrons in terms of drift resonance [e.g., *Zong et al.*, 2009], the active role of the ULF standing waves on the dynamic of ring current O^+ ions could not be omitted. Due to resonant interactions, the wave amplitudes should be decaying in event A and growing in event B. However, it is difficult to quantify this process. The wave-particle interaction is only a fraction of energy transport of ULF wave in

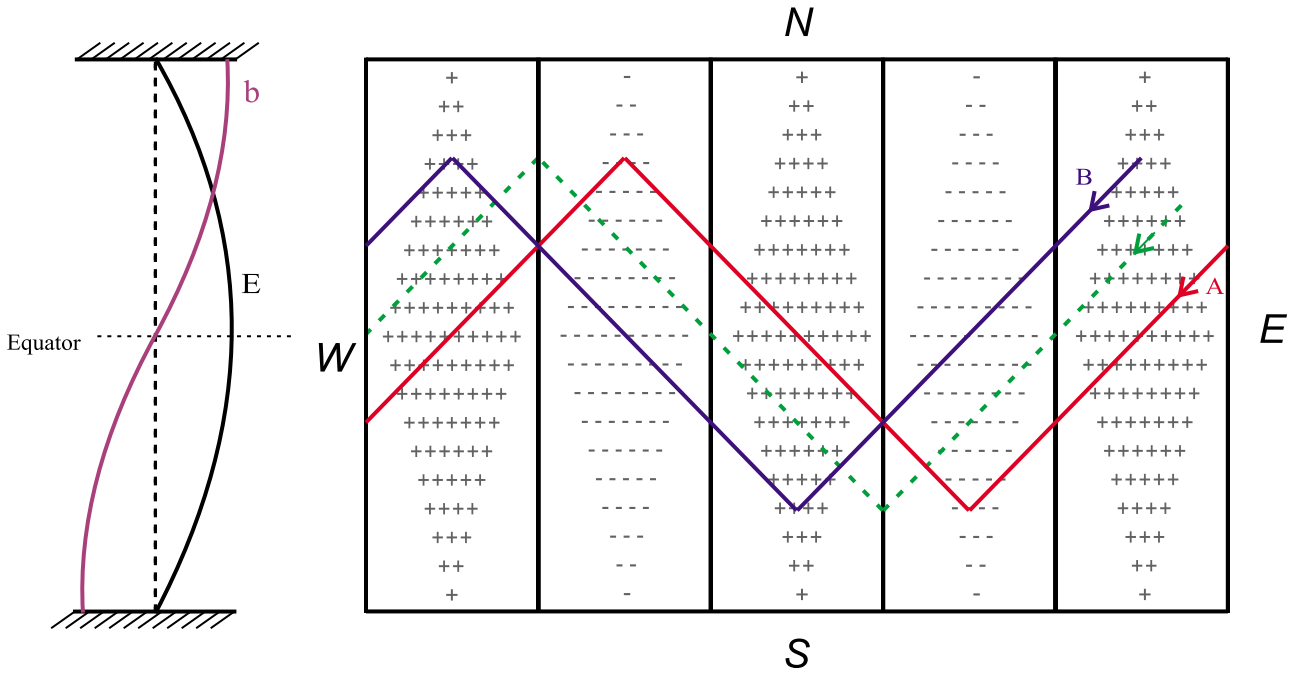

Figure 13. (right) Schematic illustration of the N = 2 drift-bounce resonance in a stretched string model viewed in the wave frame. (left) Amplitude distributions of the fundamental mode carried by the electric field (black curve) and magnetic field (purple curve) along the magnetic field line. The westward and eastward electric fields are indicated by plus and minus, and their magnitudes correspond to the density of the symbols. The colored lines represent the guiding center trajectories of O^+ ions starting at different azimuthal phases of the wave. The O^+ ions moving along the green dashed line will be accelerated and decelerated by equal strengths of westward and eastward electric field within each bounce period and get no net acceleration. The O^+ ions moving along the red and blue solid lines represent the situations of event A (25 October 2002) and event B (4 November 2002), respectively. (After *Southwood and Kivelson* [1982].)

the magnetosphere. The ULF waves could be damped and dissipate energy in the ionosphere via Joule heating [e.g., *Greenwald and Walker*, 1980; *Crowley et al.*, 1987]. In both events, the two satellites traveled across approximately the same L shell region one by one with a time lag of about 40 to 45 min. The ULF standing waves might dissipate some of energy in the ionosphere as time went by. In addition, the source stimulating the ULF wave activities could be variable. The wave signals might be even amplified due to the enhanced energy feeding from the source. Thus, we suggest that the comparison of the wave powers from the two satellites could weakly give a causal indication about the energy transfer process between the ULF waves and O^+ ions.

[44] *Li et al.* [1993] numerically studied the loss of the ring current O^+ ions at tens of keV due to their interactions with the ULF Pc5 waves via drift-bounce resonance. They pointed out that whether the O^+ ions gain or lose energy depends on their initial position with respect to the azimuthal phase of the wave. We suggest that the different behaviors of the O^+ ions in terms of acceleration in event A and deceleration in event B can be attributed to the different initial phases of the bulk of O^+ ions relative to the waves. Figure 13 gives a schematic sketch to explain the difference. We suppose the guiding center orbits of the resonant O^+ ions in event A move along the red solid line. They experience a strong accelerating electric field (westward) and a weak decelerating electric field (eastward) within each bounce period and thus get a net acceleration. While in event B, the O^+ ions are supposed to move along the blue line and finally get a net deceleration within each bounce period. The detail description of the sketch is presented in Figure 13 caption.

[45] Based on quasi-linear theory, the resonant particles will diffuse under the influence of the wave from a region of high phase space density f to a region of low f. The particles will gain a net of energy if the diffusion is toward higher energy W and vice versa [*Southwood et al.*, 1969]. In equation (5), the term $\partial f/\partial W$ are negative in both events from the spectra shown in Figures 6 and 12. The quantity dL/dW is positive for ions in eastward propagating waves. Then, the acceleration/deceleration of the O^+ ions is systematically associated with the spatial gradient, $\partial f/\partial L$. Unfortunately, this term could not be obtained directly from observations, since at least four-point measurements are required. It is inferred that the spatial gradients of f should be positive in event B might be negative in event A.

3.5. Event List

[46] The modulations of the ring current O^+ ions in periods of ULF Pc5 range are not rare. We examine the CODIF data during 2001–2005 and find 22 events in which the O^+ fluxes are distinctly modulated by ULF waves, as shown in Table 2. In some events, we find no visible magnetic/electric ULF waves at the same period as the O^+ flux oscillations.

Table 2. Summary of the O^+ Flux Modulation Events During 2001–2005

Date (yymmdd)	Time (UT)	Satellite	T_{O^+}[a] (s)	E_{O^+}[b] (keV)	MLT	L Value	ULF Wave? B[c]	ULF Wave? E[d]	*Kp*	*Dst* (nT)	Storm Phase[e]	IMF *Bz* (nT)	V_{sw} (km/s)	P_{sw} (nPa)
010923	1030–1100	C1,4	~240	15–40	1120	6.4–11.0	N	N	4.7	6	SSC	1.1	474	5.0
011021	2300–2350	C1,4	~300	2–9	0900	4.5–5.4	N	N	7.7	−180	Recovery	−15.7	639	15.0
011029	0120–0200	C1,4	~320	5–10	0820	10.5–5.8	N	N	3.3	−83	Recovery	−1.3	454	3.2
020720	0315–0340	C4	~200	9–40	1530	8.5–5.8	N	N	4.3	−15	Quiet	−4.3	898	2.3
021001	2145–2205	C1	~180	5–9	1030	5.4–4.8	N	N	6.7	−156	Recovery	−13.5	375	3.6
021006	1500–1525	C4	~300	5–40	1000	13.4–9.0	Y	N	3.3	−46	Recovery	−0.8	567	1.6
021025	1525–1645	C1,4	~290	5–40	0920	10.9–6.3	Y	Y	3.0	−72	Recovery	3.4	672	1.9
021104	0430–0540	C1,4	~270	3–25	0800	9.4–6.4	Y	Y	4.0	−69	Recovery	2.1	485	1.8
021113	1615–1645	C1,4	~300	3–40	0810	10.9–7.2	Y	Y	1.7	−25	Recovery	−0.2	567	1.2
021123	0535–0600	C4	~380	5–25	0630	10.9–6.7	Y	Y	4.3	−57	Recovery	−0.4	584	2.7
021202	1810–1840	C4	~240	9–40	0640	9.9–6.1	Y	N	3.3	−27	Recovery	−1.9	478	2.1
021207	1250–1350	C1	~240	3–10	0600	5.0–6.9	N	Y	3.3	−23	Quiet	1.4	594	5.3
021214	1505–1550	C4	~240	9–40	0610	12.8–7.1	N	N	4.0	−12	Quiet	−5.0	444	3.2
030530	0405–0525	C1,4	~270	5–25	1900	8.6–5.6	N	N	5.3	−112	Recovery	16.4	644	19.0
030919	0210–0245	C4	~200	15–40	1120	11.6–6.7	Y	Y	4.7	−41	Recovery	1.9	745	1.7
031015	1610–1640	C4	~230	5–25	0910	9.4–6.1	Y	Y	4.7	−58	Recovery	−0.4	652	2.1
031029	1230–1430	C4	~150	2–25	0850	4.3–6.8	Y	Y	7.7	−111	Recovery	13.1	X[f]	X
031031	2145–2225	C1,4	~250	5–40	0840	9.1–5.4	Y	Y	4.3	−63	Recovery	−1.5	850	3.6
031117	1230–1300	C4	~180	25–40	0740	10.3–7.2	Y	Y	4.7	−25	Recovery	−1.2	734	1.6
041110	0300–0400	C4	~150	5–25	0800	4.8–3.9	N	Y	8.3	−160	Main	−11.2	782	7.7
041201	1050–1120	C4	~200	25–40	0650	11.2–7.6	Y	Y	2.7	−32	Recovery	1.4	622	2.1
050103	1855–1910	C4	~280	10–25	0420	7.9–6.4	Y	N	3.0	−38	Recovery	0.8	651	2.4

[a]The main period of the O^+ flux oscillations.
[b]The energy range of the distinct O^+ flux oscillations.
[c]The appearance of visible magnetic field fluctuation at the same period as the O^+ fluxes.
[d]The appearance of visible electric field fluctuation at the same period as the O^+ fluxes.
[e]The storm time is defined as in the situation that appears *Dst* index less than −50 nT either 72 h before or 24 h after the time of interest.
[f]No data available.

This is probably because the satellites are located near the node of the magnetic (electric) standing wave, or the ULF waves at the modulation frequency are mixed by other wave components [e.g., *Yang et al.*, 2010].

[47] It is worth noting that the Cluster satellites are operating on a polar elliptical orbit with a period of 57 h. That makes the satellites detecting the inner magnetosphere for only about 3 h in each orbit. There should be a lot of events are missed due to the restriction of the satellite's orbit. In addition, this particular orbit also makes it hard to examine the acceleration effect of the O^+ ions via resonating with the ULF waves for a single satellite, considering the confusion of temporal effective with spatial variations. Taking advantage of multisatellite observations, we show here the two most representative events and reveal the effective role of ULF standing waves in accelerating/decelerating the ring current O^+ ions via drift-bounce resonance. Future missions such as the NASA RBSP, and the CSA ORBITALS [*Mann et al.*, 2006], which will study the radiation belt and ring current dynamics during solar maximum, are hoped to shed more light on this issue.

4. Summary

[48] We investigate the dynamics of low-energy O^+ ions (1–40 keV) in the outer ring current region in terms of their flux modulations by ULF Pc5 waves during storm times. Taking advantage of multisatellite observations by Cluster mission, we present two events occurring on the morning side of the outer ring current with radial distances of about 5.5 R_E. Distinct O^+ ion flux modulations are detected associated with fundamental mode ULF standing waves.

[49] In one event occurred on 25 October 2002, we propose the excitation of drift-bounce resonance of O^+ ions at around 20 keV with the poloidal standing wave. The theoretical estimation of the resonant energy further confirms this paradigm. Further, the O^+ spectra observed by both satellites SC1 and SC4 exhibit significant deviations from typical power law distribution at 10 to 25 keV. This can be attributed to the acceleration of O^+ ions at this energy range through wave-particle resonant interactions. In the other event occurred on 4 November 2002, we propose that the drift-bounce resonance of O^+ ions at around 7 keV are excited with both the poloidal and toroidal standing waves, as observed by satellite SC1 during strong wave activities. The O^+ spectra at 4 to 8 keV remarkably deviates the typical power law distribution. When the wave activities become rather weak as detected by satellite SC4, the O^+ spectra is found to be close to the power law distribution. The spectra comparison suggests that the O^+ at 4 to 8 keV are decelerated via drift-bounce resonances during the strong wave activities.

[50] We conclude that ring current O^+ ions with energies of several to tens of keV can be accelerated/decelerated by the ULF poloidal and toroidal standing waves during storm times.

[51] **Acknowledgments.** We thank the Cluster FGM and EFW science teams for the data used in this study. The solar wind data are obtained from the SPDF-OMNIWeb service (http://omniweb.gsfc.nasa.gov/). The *Dst* and *Kp* indexes are provided by the World Data Center for Geomagnetism, Kyoto (http://wdc.kugi.kyoto-u.ac.jp/). The authors thank A. T. Y. Lui for very helpful discussion. This work is supported by the NSFC grants 40831061 and 41074117 and Chinese Key Research Project 2011CB811404, and partly supported by the Special Fund for

Research in the Public Interest (201005017-3) and the Specialized Research Fund for State Key Laboratories.

[52] Masaki Fujimoto thanks Richard Denton, Dimitrios V. Sarafopoulos, and another reviewer for their assistance in evaluating this paper.

References

Baker, D. N., P. R. Higbie, and R. D. Belian (1980), Multispacecraft observations of energetic electron flux pulsations at 6.6 R_E, *J. Geophys. Res.*, *85*(A12), 6709–6718, doi:10.1029/JA085iA12p06709.

Balogh, A., et al. (2001), The cluster magnetic field investigation: Overview of in-flight performance and initial results, *Ann. Geophys.*, *19*, 1207–1217, doi:10.5194/angeo-19-1207-2001.

Brown, W. L., L. J. Cahill, L. R. Davis, C. E. McIlwain, and C. S. Roberts (1968), Acceleration of trapped particles during a magnetic storm on April 18, 1965, *J. Geophys. Res.*, *73*(1), 153–161, doi:10.1029/JA073i001p00153.

Chisham, G. (1996), Giant pulsations: An explanation for their rarity and occurrence during geomagnetically quiet times, *J. Geophys. Res.*, *101*(A11), 24,755–24,763, doi:10.1029/96JA02540.

Crowley, G., W. Hughes, and T. Jones (1987), Observational evidence of cavity modes in the Earth's magnetosphere, *J. Geophys. Res.*, *92*(A11), 12,233–12,240, doi:10.1029/JA092iA11p12233.

Daglis, I., and W. Axford (1996), Fast ionospheric response to enhanced activity in geospace: Ion feeding of the inner magnetotail, *J. Geophys. Res.*, *101*(A3), 5047–5065, doi:10.1029/95JA02592.

Daglis, I. A., R. M. Thorne, W. Baumjohann, and S. Orsini (1999), The terrestrial ring current: Origin, formation, and decay, *Rev. Geophys.*, *37*(4), 407–438, doi:10.1029/1999RG900009.

Delcourt, D., J. Sauvaud, and A. Pedersen (1990), Dynamics of single-particle orbits during substorm expansion phase, *J. Geophys. Res.*, *95*(A12), 20,853–20,865, doi:10.1029/JA095iA12p20853.

Elkington, S. R., M. K. Hudson, and A. A. Chan (2003), Resonant acceleration and diffusion of outer zone electrons in an asymmetric geomagnetic field, *J. Geophys. Res.*, *108*(A3), 1116, doi:10.1029/2001JA009202.

Fok, M.-C., T. E. Moore, P. C. Brandt, D. C. Delcourt, S. P. Slinker, and J. A. Fedder (2006), Impulsive enhancements of oxygen ions during substorms, *J. Geophys. Res.*, *111*, A10222, doi:10.1029/2006JA011839.

Fu, S. Y., B. Wilken, Q. G. Zong, and Z. Y. Pu (2001), Ion composition variations in the inner magnetosphere: Individual and collective storm effects in 1991, *J. Geophys. Res.*, *106*(A12), 29,683–29,704, doi:10.1029/2000JA900173.

Glassmeier, K.-H., S. Buchert, U. Motschmann, A. Korth, and A. Pedersen (1999), Concerning the generation of geomagnetic giant pulsations by drift-bounce resonance ring current instabilities, *Ann. Geophys.*, *17*, 338–350, doi:10.1007/s00585-999-0338-4.

Gloeckler, G., B. Wilken, W. Stüdemann, F. M. Ipavich, D. Hovestadt, D. C. Hamilton, and G. Kremser (1985), First composition measurement of the bulk of the storm-time ring current (1 to 300 keV/e) with AMPTE-CCE, *Geophys. Res. Lett.*, *12*(5), 325–328, doi:10.1029/GL012i005p00325.

Greenwald, R. A., and A. D. M. Walker (1980), Energetics of long period resonant hydromagnetic waves, *Geophys. Res. Lett.*, *7*(10), 745–748, doi:10.1029/GL007i010p00745.

Grinsted, A., J. C. Moore, and S. Jevrejeva (2004), Application of the cross wavelet transform and wavelet coherence to geophysical time series, *Nonlinear Process. Geophys.*, *11*, 561–566, doi:10.5194/npg-11-561-2004.

Gustafsson, G., et al. (2001), First results of electric field and density observations by Cluster EFW based on initial months of operation, *Ann. Geophys.*, *19*, 1219–1240, doi:10.5194/angeo-19-1219-2001.

Hamilton, D. C., G. Gloeckler, and F. M. Ipavich (1988), W. Stdemann, B. Wilken, and G. Kremser, Ring current development during the great geomagnetic storm of February 1986, *J. Geophys. Res.*, *93*(A12), 14,343–14,355, doi:10.1029/JA093iA12p14343.

Hamlin, D. A., R. Karplus, R. C. Vik, and K. M. Watson (1961), Mirror and azimuthal drift frequencies for geomagnetically trapped particles, *J. Geophys. Res.*, *66*, 1–4, doi:10.1029/JZ066i001p00001.

Hughes, W. J., D. J. Southwood, B. Mauk, R. L. McPherron, and J. N. Barfield (1978), Alfven waves generated by an inverted plasma energy distribution, *Nature*, *275*, 43–45, doi:10.1038/275043a0.

Ipavich, F., A. Galvin, M. Scholer, G. Gloeckler, D. Hovestadt, and B. Klecker (1985), Suprathermal O+ and H+ ion behavior during the March 22, 1979 (CDAW 6), substorms, *J. Geophys. Res.*, *90*(A2), 1263–1272, doi:10.1029/JA090iA02p01263.

Kamide, Y., et al. (1998), Current understanding of magnetic storms: Storm-substorm relationships, *J. Geophys. Res.*, *103*, 17,705–17,728, doi:10.1029/98JA01426.

Kokubun, S., M. G. Kivelson, R. L. McPherron, C. T. Russell, and H. I. West Jr. (1977), Ogo 5 observations of Pc 5 waves: Particle flux modulations, *J. Geophys. Res.*, *82*(19), 2774–2786, doi:10.1029/JA082i019p02774.

Kremser, G., A. Korth, J. A. Fejer, B. Wilken, A. V. Gurevich, and E. Amata (1981), Observations of quasi-periodic flux variations of energetic ions and electrons associated with Pc 5 geomagnetic pulsations, *J. Geophys. Res.*, *86*(A5), 3345–3356, doi:10.1029/JA086iA05p03345.

Krimigis, S. M., G. Gloeckler, R. W. McEntire, T. A. Potemra, F. L. Scarf, and E. G. Shelley (1985), Magnetic storm of September 4, 1984: A synthesis of ring current spectra and energy densities measured with AMPTE/CCE, *Geophys. Res. Lett.*, *12*(5), 329–332, doi:10.1029/GL012i005p00329.

Li, X., M. Hudson, A. Chan, and I. Roth (1993), Loss of ring current O+ ions due to interaction with Pc 5 waves, *J. Geophys. Res.*, *98*(A1), 215–231, doi:10.1029/92JA01540.

Mann, I. R., et al. (2006), The outer radiation belt injection, transport, acceleration and loss satellite (ORBITALS): A Canadian small satellite mission for ILWS, *Adv. Space Res.*, *38*, 1838–1860, doi:10.1016/j.asr.2005.11.009.

Maynard, N., and A. Chen (1975), Isolated cold plasma regions: Observations and their relation to possible production mechanisms, *J. Geophys. Res.*, *80*(7), 1009–1013, doi:10.1029/JA080i007p01009.

McIlwain, C. E. (1961), Co-ordinates for mapping the distributions of magnetically trapped particles, *J. Geophys. Res.*, *66*, 3681–3691, doi:10.1029/JZ066i011p03681.

Nosé, M., A. T. Y. Lui, S. Ohtani, B. H. Mauk, R. W. McEntire, D. J. Williams, T. Mukai, and K. Yumoto (2000), Acceleration of oxygen ions of ionospheric origin in the near-Earth magnetotail during substorms, *J. Geophys. Res.*, *105*(A4), 7669–7678, doi:10.1029/1999JA000318.

Nosé, M., S. Taguchi, K. Hosokawa, S. P. Christon, R. W. McEntire, T. E. Moore, and M. R. Collier (2005), Overwhelming O^+ contribution to the plasma sheet energy density during the October 2003 superstorm: Geotail/EPIC and IMAGE/LENA observations, *J. Geophys. Res.*, *110*, A09S24, doi:10.1029/2004JA010930.

Nosé, M., S. Taguchi, S. P. Christon, M. R. Collier, T. E. Moore, C. W. Carlson, and J. P. McFadden (2009), Response of ions of ionospheric origin to storm time substorms: Coordinated observations over the ionosphere and in the plasma sheet, *J. Geophys. Res.*, *114*, A05207, doi:10.1029/2009JA014048.

Ozeke, L. G., and I. R. Mann (2008), Energization of radiation belt electrons by ring current ion driven ULF waves, *J. Geophys. Res.*, *113*, A02201, doi:10.1029/2007JA012468.

Rème, H., et al. (2001), First multispacecraft ion measurements in and near the Earth's magnetosphere with the identical Cluster Ion Spectrometry (CIS) experiment, *Ann. Geophys.*, *19*, 1303–1354, doi:10.5194/angeo-19-1303-2001.

Sánchez, E. R., B. H. Mauk, and C. I. Meng (1993), Adiabatic vs. non-adiabatic particle distributions during convection surges, *Geophys. Res. Lett.*, *20*(3), 177–180, doi:10.1029/93GL00237.

Sarafopoulos, D., N. Sidiropoulos, E. Sarris, V. Lutsenko, and K. Kudela (2001), The dawn-dusk plasma sheet asymmetry of energetic particles: An Interball perspective, *J. Geophys. Res.*, *106*(A7), 13,053–13,065, doi:10.1029/2000JA900157.

Singer, H. J., W. J. Hughes, and C. T. Russell (1982), Standing hydromagnetic waves observed by ISEE 1 and 2: Radial extent and harmonic, *J. Geophys. Res.*, *87*, 3519–3529, doi:10.1029/JA087iA05p03519.

Southwood, D. J., and M. G. Kivelson (1981), Charged particle behavior in low-frequency geomagnetic pulsations: 1. Transverse waves, *J. Geophys. Res.*, *86*(A7), 5643–5655, doi:10.1029/JA086iA07p05643.

Southwood, D. J., and M. G. Kivelson (1982), Charged particle behavior in low-frequency geomagnetic pulsations: 2. Graphical approach, *J. Geophys. Res.*, *87*(A3), 1707–1710, doi:10.1029/JA087iA03p01707.

Southwood, D. J., J. W. Dungey, and R. J. Etherington (1969), Bounce resonant interaction between pulsations and trapped particles, *Planet. Space Sci.*, *17*, 349–361, doi:10.1016/0032-0633(69)90068-3.

Stern, D. (1975), The motion of a proton in the equatorial magnetosphere, *J. Geophys. Res.*, *80*(4), 595–599, doi:10.1029/JA080i004p00595.

Su, S. Y., R. L. McPherron, A. Konradi, and T. A. Fritz (1980), Observations of ULF oscillations in the ion fluxes at small pitch angles with ATS 6, *J. Geophys. Res.*, *85*(A2), 515–522, doi:10.1029/JA085iA02p00515.

Takahashi, K., and A. Y. Ukhorskiy (2007), Solar wind control of Pc5 pulsation power at geosynchronous orbit, *J. Geophys. Res.*, *112*, A11205, doi:10.1029/2007JA012483.

Takahashi, K., P. R. Higbie, and D. N. Baker (1985), Energetic electron flux pulsations observed at geostationary orbit: Relation to magnetic pulsations, *J. Geophys. Res.*, *90*(A9), 8308–8318, doi:10.1029/JA090iA09p08308.

Takahashi, K., R. W. McEntire, A. T. Y. Lui, and T. A. Potemra (1990), Ion flux oscillations associated with a radially polarized transverse Pc 5 magnetic pulsation, *J. Geophys. Res.*, *95*(A4), 3717–3731, doi:10.1029/JA095iA04p03717.

Volland, H. (1973), A semiempirical model of large-scale magnetospheric electric fields, *J. Geophys. Res.*, *78*(1), 171–180, doi:10.1029/JA078i001p00171.

Wilken, B., Q. G. Zong, I. A. Daglis, T. Doke, S. Livi, K. Maezawa, Z. Y. Pu, S. Ullaland, and T. Yamamoto (1995), Tailward flowing energetic oxygen ion bursts associated with multiple flux ropes in the distant magnetotail: GEOTAIL observations, *Geophys. Res. Lett.*, *22*(23), 3267–3270, doi:10.1029/95GL02980.

Wilken, B., et al. (2001), First results from the RAPID imaging energetic particle spectrometer on board Cluster, *Ann. Geophys.*, *19*, 1355–1366, doi:10.5194/angeo-19-1355-2001.

Williams, D. J. (1981), Ring current composition and sources: An update, *Planet. Space Sci.*, *29*, 1195–1203, doi:10.1016/0032-0633(81)90124-0.

Williams, D. J. (1983), The Earth's ring current: Causes, generation, and decay, *Space Sci. Rev.*, *34*, 223–234, doi:10.1007/BF00175279.

Williams, D. J. (1985), Dynamics of the Earth's ring current: Theory and observation, *Space Sci. Rev.*, *42*, 375–396, doi:10.1007/BF00214994.

Wright, D. M., T. K. Yeoman, I. J. Rae, J. Storey, A. B. Stockton-Chalk, J. L. Roeder, and K. J. Trattner (2001), Ground-based and Polar spacecraft observations of a giant (Pg) pulsation and its associated source mechanism, *J. Geophys. Res.*, *106*(A6), 10,837–10,852, doi:10.1029/2001JA900022.

Yang, B., Q. G. Zong, Y. F. Wang, S. Y. Fu, P. Song, H. S. Fu, A. Korth, T. Tian, and H. Reme (2010), Cluster observations of simultaneous resonant interactions of ULF waves with energetic electrons and thermal ion species in the inner magnetosphere, *J. Geophys. Res.*, *115*, A02214, doi:10.1029/2009JA014542.

Yang, B., et al. (2011), Pitch angle evolutions of oxygen ions driven by storm-time ULF poloidal standing waves, *J. Geophys. Res.*, doi:10.1029/2010JA016047, in press.

Zong, Q., et al. (1997), Geotail observations of energetic ion species and magnetic field in plasmoid-like structures in the course of an isolated substorm event, *J. Geophys. Res.*, *102*(A6), 11,409–11,428, doi:10.1029/97JA00076.

Zong, Q., et al. (1998), Energetic oxygen ion bursts in the distant magnetotail as a product of intense substorms: Three case studies, *J. Geophys. Res.*, *103*(A9), 20,339–20,363, doi:10.1029/97JA01146.

Zong, Q.-G., B. Wilken, S. Fu, T. Fritz, A. Korth, N. Hasebe, D. Williams, and Z.-Y. Pu (2001), Ring current oxygen ions escaping into the magnetosheath, *J. Geophys. Res.*, *106*(A11), 25,541–25,556, doi:10.1029/2000JA000127.

Zong, Q.-G., et al. (2007), Ultralow frequency modulation of energetic particles in the dayside magnetosphere, *Geophys. Res. Lett.*, *34*, L12105, doi:10.1029/2007GL029915.

Zong, Q.-G., H. Zhang, S. Y. Fu, Y. F. Wang, Z. Y. Pu, A. Korth, P. W. Daly, and T. A. Fritz (2008), Ionospheric oxygen ions dominant bursty bulk flows: Cluster and Double Star observations, *J. Geophys. Res.*, *113*, A07S23, doi:10.1029/2007JA012764.

Zong, Q.-G., et al. (2009), Energetic electrons response to ULF waves induced by interplanetary shocks in the outer radiation belt, *J. Geophys. Res.*, *114*, A10204, doi:10.1029/2009JA014393.

H. S. Fu, Space Science Institute, School of Astronautics, Beihang University, Beijing 100191, China.

S. Y. Fu, B. Yang, C. Yue, and Q.-G. Zong, Institute of Space Physics and Applied Technology, Peking University, Beijing 100871, China. (yangbiao@pku.edu.cn)

A. Korth, Max-Planck Institute for Solar System Research, D-37191, Katlenburg-Lindau, Germany.

X. Li, Laboratory for Atmospheric and Space Physics, University of Colorado, 1234 Innovation Drive, Boulder, CO 80303, USA.

H. Reme, University of Toulouse, UPS, CESR, 9 av. du Colonel Roche, F-31028, Toulouse CEDEX 4, France.